Effect of a vortex in the triply differential cross section for electron-impact *K*-shell ionization of carbon

S. J. Ward*
Department of Physics, University of North Texas, Denton, Texas 76203, USA

J. H. Macek
Department of Physics and Astronomy, University of Tennessee, Knoxville, Tennessee 37996, USA

(Received 21 May 2014; revised manuscript received 2 September 2014; published 12 December 2014)

Vortices are an inherent property of the velocity fields of complex, time-dependent, Schrödinger wave functions ψ occurring where both the real and the imaginary parts of ψ vanish. They have been known since the early work of Dirac on magnetic monopoles and have frequently been studied theoretically. The possibility of observing them by exploiting an "imaging theorem" that relates atomic wave functions to measured electron momentum distributions has recently been proposed. Using the Coulomb-Born approximation, we examine ionization of a *K*-shell electron of a model carbon atom by fast electron impact. For an incident electron energy of 1801.2 eV and a scattering angle of 4°, we find a vortex in the velocity field associated with a zero in the ionization *T*-matrix element and hence in the triply differential cross section, and we obtain a segment of the vortex line. Angular momentum transfer is essential to produce the vortex in the velocity field and the corresponding zero in the ionization *T*-matrix element and in the triply differential cross section.

DOI: 10.1103/PhysRevA.90.062709 PACS number(s): 34.80.Dp

I. INTRODUCTION

High-energy limits of atomic scattering processes are of interest because the theory of such processes is often amenable to quantitative, even closed-form, treatments. Indeed, the high-energy theories of atomic collisions and energy loss in matter are based on the first Born (B1) approximations [1–3]. The Born and higher-order approximations have also been used extensively to interpret structures in the electron momentum distributions produced in ion and electron impact on neutral atoms [2,4]. It was speculated that all structures seen in such distributions arise from the first or second Born terms in the ionization *T*-matrix element [4]. It was later recognized that certain minima found by Murray and Read [5,6] in $(e,2e)$ electron distributions did not follow the usual pattern of structures in momentum distributions. Usually, a two-dimensional slice through a three-dimensional electron momentum distribution will exhibit minima in the form of nodal lines, whereas the minima in Refs. [5] and [6] were found at isolated points on a two-dimensional surface [7,8]. It was later found that these isolated zeros relate to vortices in the velocity field of atomic wave functions for the $(e,2e)$ process [9]. Accurate values for these zeros were computed by Colgan *et al.* [10] and were discussed by Feagin [11]. A sharp minimum in the triply differential cross section (TDCS) has been predicted by Colgan *et al.* [10] for electron-impact ionization of molecular hydrogen with a specific orientation. Vortices have been considered for ionization by proton impact in a number of places [12–21], including Ref. [14], which connects time-dependent theory with time-independent theory. Vortices have also been obtained in ionization by He^{2+} ions [22] and by antiproton impact [21] as well as in photoionization [21]. A vortex recently obtained for positron-impact ionization of hydrogen [23,24] provided an explanation of a deep minimum in a fully differential cross section previously obtained [25]. The creation of vortices has been demonstrated in the electronic probability density of an atom subject to short electric field pulses [20,26]. Vortices are also of interest in other area of physics, such as in exciton-polariton condensates [27].

For ionization of a *K*-shell electron of a model carbon atom by fast electron impact using the Coulomb-Born approximation given by Botero and Macek [28], we find a zero in the ionization *T*-matrix element and in the TDCS [29]. The zero corresponds to a vortex in the velocity field associated with the *T*-matrix element for ionization. In Sec. II we review and discuss vortices in velocity fields. In Sec. III we give the position of the zero we find in the *T*-matrix element and give a segment of the vortex line. For ionization by a charged particle, transfer of the vector angular momentum is associated with an isolated zero in the time-dependent wave function of an ejected electron at an asymptotic distance [9,13,21,25]. The connection between a simple analytic property of an atomic wave function and the transfer of angular momentum has been previously discussed [9,13–15,17,18,21,22,26,30].

Isolated zeros can occur in pairs. In this case the net angular momentum transfer may be zero. Bialynicki-Birula *et al.* [31] considered a vortex pair where the two lines have opposite circulation and they also considered ring vortices. We note that, using the time-dependent Schrödinger equation, Bialynicki-Birula *et al.* obtained a rectilinear vortex for a particle in a uniform magnetic field. In our work we do not consider magnetic fields. Using both the time-dependent Schrödinger equation and the Klein-Gordon equation, Bialynicki-Birula *et al.* also obtained a rectilinear vortex for a free particle. Previously, Fetter [32] obtained a single vortex for a one-particle wave function that satisfies a time-dependent nonlinear equation.

The B1, distorted-wave Born (DWB), and Coulomb-Born approximations are considered valid when the relative velocities $\mathbf{v}$ of the colliding particles are high compared with the mean velocities of the active electrons [3]. This high-velocity requirement is well established but must be understood in

*Corresponding author: sward@unt.edu

the correct sense, usually in the sense that the momentum $\boldsymbol{K}$ transferred from relative to internal motion is held constant. Derivations, originating with Henneberg [33] and Livingston and Bethe [34], have articulated a wider application of the B1 theory based on an expansion of transition amplitudes in terms of ratios of the charge of the projectile Z_P relative to the charge of the target Z_T [3,28,35–39]. Such expansions are less well known than expansions in velocity ratios, however, they are related to the B1 theory by standard approximations.

Some of these approximations apply to high-energy limits taken holding the scattering angle θ_f fixed [40,41]. In that case, amplitudes for inelastic transitions are given by some sort of distorted-wave approximation which allows for the scattering of the incident projectile P from the target T. For fixed *scattering angle* θ_f and definite energy loss, the momentum $\boldsymbol{K}$ lost by the projectile increases without limit so that the scattering is mainly between the atomic nuclei and the projectile as in Rutherford's measurements. Indeed, the amplitude for elastic scattering becomes just the Rutherford scattering amplitude. For inelastic transitions the change of state of the electrons is a small perturbation to the Coulomb scattering from the target nucleus. In this case the Coulomb-Born approximation is a logical limit, comparable to the Born approximation relevant at fixed momentum transfer. For the Coulomb-Born approximation, not only is linear momentum transfer relevant, but also angular momentum transfer occurs [39], something that does happen when the limit is taken holding $\boldsymbol{K}$ constant. We use the theory given in Ref. [28], which shows how Coulomb waves moving in arbitrary point charge potentials can be employed in a consistent perturbation expansion so that all orders in the perturbation expansion are finite. The Coulomb-Born theory describes excitation and ionization at high energies when the limit is taken holding the scattering angle constant. In this limit the excited states could also be oriented. Indeed, this was shown in Ref. [39] for the excitation of p states in collisions of electrons with ground-state He^+ ions.

The interpretation of angular momentum transfer is usually given in terms of the alignment and orientation anisotropy parameters of Fano and Macek [42–45]. The orientation parameter, given by the mean value of the angular momentum $\langle J_z \rangle$, is known to be relevant for excitation of bound states [45]. It has recently been discovered that orientation of continuum states by atomic collisions leads to zeros in the angular distribution of ionized electrons [12,13,15]. Since these are also zeros in the wave function at large values of the electron coordinate, they also correspond to vortices in the velocity field. In essence, it is found that transfer of angular momentum involves two rotations [14]. One rotation is the normal classical picture of orbiting about a charge center or, in the language of quantum mechanics, the rotation of a bound electron's probability distribution as a whole about a charge center. A second rotation is a rotation about a zero of the electron wave function [13,14,21]. It has been shown that if a complex one-electron wave function has an isolated zero, the zero corresponds to vortex in the velocity field [31,46,47]. This implies that the probability current circulates about the isolated zero and becomes infinite exactly at the vortex. The integral of the current around the vortex is some integer multiple of 2π [31]. It is established for proton impact ionization that vortices corresponding to zeros in the time-dependent electron wave function show up as zeros in the electron momentum distribution of the ejected electrons $\boldsymbol{k}$ [13,14].

In Sec. III we show that a vortex occurs for inner-shell ionization by electron impact using the Coulomb-Born approximation given by Botero and Macek [28]. We review the Coulomb-Born approximation that was applied in Ref. [28] to ionization of a K-shell electron of a carbon atom by fast electron impact and which uses an effective charge $Z_{\rm eff}$ not equal to the charge of the target nucleus. For the process of electron K-shell ionization of a model carbon atom, we give the kinematics for a vortex in the velocity field that manifests itself as a deep minimum in the TDCS and we also provide verification of the vortex [29]. We also give a multipole expansion of the Coulomb-Born ionization T-matrix element for the kinematics of the vortex and analyze the multipoles to determine the most important components necessary to obtain a vortex. We also give in Sec. III the loci of points where a vortex appears in the velocity field when the electron is ejected out of the scattering plane. Previously, minima in the TDCS for inner-shell ionization of carbon [28] have been attributed to vortices and an analysis had been made using the multipole components [9,14,17,18] computed by Botero and Macek [28]. The kinematics for the minima in the TDCS in Ref. [28], however, are generally close to the kinematics for a vortex in the velocity field rather than exactly at the kinematics for a vortex.

We present a summary in Sec. IV and in the Appendix we give the corrected analytic expression for the multipole components of the ionization T-matrix element for the Born approximation that were given in Ref. [28], but apparently with some errors.

Atomic units are used throughout unless explicitly stated otherwise.

II. VORTICES IN VELOCITY FIELDS OF ATOMIC WAVE FUNCTIONS

Vortices in the velocity fields of atomic wave functions have been discussed generally by Bialynicki-Birula *et al.* [31], where they have been related to local rotational properties near isolated zeros of one-electron atomic wave functions. In this section we review some central features of vortices of velocity fields given in Ref. [31].

Consider a complex function $f(x,y)$ in two dimensions whose Cartesian coordinates are denoted x,y. This function may vanish at the point x_0, y_0, where the real and imaginary parts of f both vanish. The function is assumed to be analytic in a region including the zero. The squared magnitude $|f(x,y)|^2$ defines the probability density, and the expression

$$\boldsymbol{v}(x,y) = \frac{\mathrm{Re}[f^*(x,y)(-i)\boldsymbol{\nabla} f(x,y)]}{|f(x,y)|^2} = \mathrm{Im}\boldsymbol{\nabla}[\ln f(x,y)] \quad (1)$$

defines the velocity field [31]. In the absence of external fields, the velocity field is irrotational $\boldsymbol{\nabla} \times \boldsymbol{v}(x,y) = 0$ except at the zero of the function $f(x,y)$, i.e., at (x_0,y_0). The function $f(x,y)$ near its zero can be taken to have the form

$$f(x,y) \approx a[(x - x_0) + b(y - y_0)], \quad (2)$$

where b is a complex number which may be time dependent and in which $\mathrm{Im}[b] \neq 0$ [9,30,31,46,48,49]. The velocity field $\boldsymbol{v}$ near the zero of this function f can be closely approximated

by its dominant term:

$$\boldsymbol{v} \approx -\mathrm{Im[b]}\frac{[\hat{x}(y-y_0)-\hat{y}(x-x_0)]}{(x-x_0)^2+|b|^2(y-y_0)^2+2\mathrm{Re[b]}(x-x_0)(y-y_0)}. \tag{3}$$

The dominant term is orthogonal to the vector $\boldsymbol{r}-\boldsymbol{r}_0$. The magnitude of the velocity field has a $1/r$ singularity at the zero of the function (x_0,y_0), where $r=\sqrt{(x-x_0)^2+(y-y_0)^2}$ [46]. Using the right-hand side of Eq. (3) and taking a circular contour c of small radius of counterclockwise orientation, enclosing the point (x_0,y_0), one can show that [9,14,30–32,46–54]

$$\int_c \boldsymbol{v}\cdot d\boldsymbol{\ell} = 2\pi. \tag{4}$$

This result, that the line integral of the velocity field $\boldsymbol{v}$ equals 2π, is true for any contour of counterclockwise orientation enclosing the first-order zero of $f(x,y)$ at (x_0,y_0), provided, of course, that there are no other zeros of the function $f(x,y)$ enclosed in the contour.

For a function $f(x,y)$ with a first-order zero, the equation $\mathrm{Re}[f(x,y)]=0$ in general defines a nodal line. The vanishing of $\mathrm{Im}[f(x,y)]=0$ similarly defines a second, generally different, nodal line. If these two nodal lines do not coincide, then where they cross defines an isolated first-order zero of the complex function $f(x,y)$ [31]. We use this procedure to locate a zero in the T-matrix element for fast electron-impact ionization of a K-shell electron of carbon. We give the position of the zero in Sec. III.

Equation (4) shows that the velocity field circulates around the zero of the function $f(x,y)$, suggesting that the velocity field carries angular momentum. Using Eq. (2) for the function $f(x,y)$ in the vicinity of the zero and averaging the z component of the angular momentum vector L_z over a small region A including the zero, one obtains [30]

$$\langle L_z\rangle = \frac{\int_A f^*(x,y)L_z f(x,y)dxdy}{\int_A |f(x,y)|^2 dxdy} \approx \frac{i(b^*-b)}{|1|^2+|b|^2}, \tag{5}$$

which is nonzero since $\mathrm{Im}[b]\neq 0$. Thus, there is some angular momentum associated with the zero of the function $f(x,y)$ given by Eq. (2).

The general theory of Ref. [31] discussed situations where the vortices occur in pairs with opposite and presumably equal magnitude currents so that the total angular momentum carried by the function f vanishes. Those situations are applicable to time-dependent wave functions prepared by processes that transfer no net vector angular momentum, like atomic excitation by linearly polarized light [26]. For ionization of a K-shell electron of carbon by fast electron impact, transfer of angular momentum is associated with the zero in the T-matrix element we obtain and present in Sec. III. We show in Sec. III that the $m=1$ dipole component of a multipole expansion of the ionization T-matrix element is necessary to obtain the zero.

That vortices, even in "fluids" that are generally irrotational such as those appropriate for time-dependent atomic wave functions [13,31,47,55,56], should have observable consequences is an important point introduced in Ref. [31]. The consequences have proved experimentally elusive, mainly since direct observation of wave functions is seldom considered as a goal for experimental or theoretical investigation. For time-dependent processes one can use that the wave function

$$\psi(\boldsymbol{r},t) = \int K(\boldsymbol{r},t;\boldsymbol{r}',t')\psi(\boldsymbol{r}',t')d^3r', \tag{6}$$

where K is the propagator or time-dependent Green's function. Upon setting $\boldsymbol{r}=\boldsymbol{k}t$ [13] and taking the limit as $t\to\infty$ one has that all bound-state components vanish since $r\to\infty$, leaving only continuum components. For sufficiently large r' the propagator can be taken to be the free particle propagator to the extent that continuum components can be represented by plane waves. In this case the propagator becomes

$$K(\boldsymbol{r},t;\boldsymbol{r}',t') = \left(\frac{1}{2\pi|t-t'|}\right)^{3/2}\exp\left[-i\frac{(\boldsymbol{r}-\boldsymbol{r}')^2}{2|t-t'|}\right]. \tag{7}$$

Upon setting $\boldsymbol{r}=\boldsymbol{k}t$ in Eq. (7) and taking the limit as $t\to\infty$ one obtains

$$\begin{aligned} K(\boldsymbol{k}t,t;\boldsymbol{r}',t') &= \left(\frac{1}{2\pi t}\right)^{3/2}\exp\left[-i\frac{(\boldsymbol{k}t-\boldsymbol{r}')^2}{2|t-t'|}\right] \\ &\to \left(\frac{1}{2\pi t}\right)^{3/2} e^{-ik^2t/2}e^{i\boldsymbol{k}\cdot\boldsymbol{r}'}. \end{aligned} \tag{8}$$

It follows that in the limit of large t one has

$$\begin{aligned} &[|\psi(\boldsymbol{r},t)|^2 d^3r]_{\boldsymbol{r}=\boldsymbol{k}t} \\ &\sim \left| d^3k\, e^{-ik^2t/2}(2\pi)^{-3/2}\int e^{i\boldsymbol{k}\cdot\boldsymbol{r}'}\psi(\boldsymbol{r}',t')d^3r'\right|^2 \\ &= |\tilde{\psi}(\boldsymbol{k},t')|^2 d^3k \propto |T_{\boldsymbol{k}}(t)|^2 d^3k, \end{aligned} \tag{9}$$

which identifies the time-dependent wave function with the momentum distribution of the ejected electron. Equation (9) is referred to as the "imaging theorem" but the identification [9,14,17,18,57–61] is usually implicitly assumed when needed. Reference [58] gives the relation $T_{\boldsymbol{k}}(t)\propto\tilde{\psi}(\boldsymbol{k},t)$, where $T_{\boldsymbol{k}}(t)$ is the time-dependent transition matrix element. We can therefore use the ionization T-matrix element to compute the velocity field. Since the imaging theorem relates an electron momentum distribution to an electron wave function, one can identify an isolated zero in an ionization T-matrix element with a vortex in a velocity field. The vortex indicates transfer of angular momentum.

It is somewhat remarkable that an analytic feature of a wave function, namely, an isolated zero, relates closely to the transfer of angular momentum. In essence, while an isolated zero of a time-dependent atomic wave function seems to be a simple analytic feature expected to be present for general functions, that is not actually the case.

In the next section we obtain a vortex for the particular process of ionization of a K-shell electron of a carbon atom by fast electron impact using the Coulomb-Born approximation given in Ref. [28] and a hydrogenic wave function for the K-shell electron as done in Ref. [28].

III. COULOMB-BORN CALCULATIONS OF ELECTRON-IMPACT IONIZATION OF THE K SHELL OF A MODEL CARBON ATOM

A. Coulomb-Born ionization T-matrix element

The Coulomb-Born (CB1) limit was studied by Botero and Macek [28] for the special case of inner-shell ionization of a carbon atom by electron impact, where Rutherford scattering by the carbon nuclei played an important role. A simple screened charge model gave an ejected electron distribution [28] in moderately good agreement with measurement [62] for the kinematics of an incident electron E_i of 1801.2 eV, a scattering angle θ_f of 4°, and an ejected electron energy $E_{\boldsymbol{k}}$ of 9.6 eV. In Refs. [9,14,17] and [18] some of the minima in the CB1 TDCSs of Botero and Macek [28] for different kinematical conditions are interpreted in terms of vortices. In this paper we discuss that the minimum in the CB1 TDCS at 240° computed by Botero and Macek for the kinematics $E_i = 1801.2$ eV, $\theta_f = 4°$, and $E_{\boldsymbol{k}} = 9.6$ eV is due to the kinematics being close to that to obtain a vortex in the velocity field rather than the kinematics for a vortex. By varying the energy of the ejected electron, we obtain a deep minimum in the CB1 TDCS which is due to a vortex.

For K-shell ionization of carbon by electron impact where a one-electron model is taken to represent the inner 1s electron in the initial state, the CB1 ionization T-matrix element has the form [28]

$$T_{fi}^{\mathrm{CB1}} = \langle \psi_{\boldsymbol{K}_f}^{-}(\boldsymbol{r})\psi_{\boldsymbol{k}}^{-}(\boldsymbol{r}')\left|\frac{1}{|\boldsymbol{r}-\boldsymbol{r}'|}\right|\varphi_i(\boldsymbol{r}')\psi_{\boldsymbol{K}_i}^{+}(\boldsymbol{r})\rangle. \tag{10}$$

In this equation, $\boldsymbol{r}$ and $\boldsymbol{r}'$ are, respectively, the position vectors of the incident (or scattered) electron and of the atomic (or ejected) electron relative to the target nucleus. In the treatment in Ref. [28] and followed here, the inner 1s electron in the initial state is approximated by a ground-state hydrogenic wave function $\varphi_i(\boldsymbol{r}') = (1/\sqrt{\pi})Z_T^{3/2}e^{-Z_T r'}$, with the screened target charge Z_T chosen so that it gives the binding energy of the 1s electron. In our calculations we take $Z_T = 4.6717$, obtained using the relaxed-orbital total binding energy of −10.912347 a.u. of the electron in the level $1S_{\frac{1}{2}}$ of carbon [63]. The ± sign on the Coulomb wave functions $\psi_{\boldsymbol{K}_f}^{-}(\boldsymbol{r})$, $\psi_{\boldsymbol{k}}^{-}(\boldsymbol{r}')$, and $\psi_{\boldsymbol{K}_i}^{+}(\boldsymbol{r})$ refer to incoming (−) and outgoing (+) boundary conditions [64], and $\boldsymbol{K}_i$, $\boldsymbol{K}_f$, and $\boldsymbol{k}$ denote the momentum of the incident, scattered, and ejected electrons, respectively. We use the normalization of the Coulomb waves on the momentum scale [28,64]. As done by Botero and Macek [28], we set the effective charge Z_{eff} in the Coulomb wave functions for the incident and scattered electron to equal Z_T.

Following through the analysis in Ref. [28] enables the CB1 ionization T-matrix element to be expressed as a two-dimensional integral,

$$T_{k,1s}^{\mathrm{CB1}} = 2\pi\frac{N_{\boldsymbol{K}_i}^{(+)}N_{\boldsymbol{K}_f}^{(-)^*}N_{\boldsymbol{k}}^{(-)^*}}{\Gamma(1-c)\Gamma(c)}\left(\frac{Z_T^3}{\pi}\right)^{1/2}\int_0^1 dt\, t^{c-1}(1-t)^{-c} \times\int_0^1 dx\left[-\frac{\mu(1-x)}{y^3}\frac{\partial I_{ab}}{\partial y}+\frac{1}{y}\frac{\partial^2 I_{ab}}{\partial y\partial\mu}\right], \tag{11}$$

where $N_{\boldsymbol{K}_i}^{+}$, $N_{\boldsymbol{K}_f}^{-}$, and $N_{\boldsymbol{k}}^{-}$ are the normalization of the Coulomb wave functions $\psi_{\boldsymbol{K}_i}^{+}(\boldsymbol{r})$, $\psi_{\boldsymbol{K}_f}^{-}(\boldsymbol{r})$, and $\psi_{\boldsymbol{k}}^{-}(\boldsymbol{r}')$, respectively. In Eq. (11), $a = i\frac{Z_{\mathrm{eff}}}{K_i}$, $b = i\frac{Z_{\mathrm{eff}}}{K_f}$, $c = i\frac{Z_T}{k}$, $\mu = Z_T - ikt$, $p = (1-x)(1-t)$, and $y = [(1-x)(\mu^2 + xp_1^2)]^{1/2}$, where $\boldsymbol{p}_1 = \boldsymbol{k}(t-1)$. As defined in Ref. [39], I_{ab} is given by

$$I_{ab} = \frac{4\pi C^{a+b-1}}{A^b B^a}{}_2F_1(a,b,1;z), \tag{12}$$

where

$$\begin{aligned} A &= (y - iK_f)^2 + (p\boldsymbol{k} - \boldsymbol{K}_i)^2,\\ B &= (y - iK_i)^2 + (p\boldsymbol{k} + \boldsymbol{K}_f)^2,\\ C &= y^2 + (p\boldsymbol{k} - \boldsymbol{K}_i + \boldsymbol{K}_f)^2,\\ D &= [y - i(K_i + K_f)]^2 + p^2k^2,\\ z &= 1 - \frac{CD}{AB}. \end{aligned} \tag{13}$$

Equations (11) and (13) correct minor mistakes in Eqs. (54) and (53) in Ref. [28], respectively.

It is useful to note the invariance of $T_{\boldsymbol{k},1s}^{\mathrm{CB1}}$ under reflection in the plane of $\boldsymbol{K}_i$ and $\boldsymbol{K}_f$ called the scattering plane. Since the vectors $\boldsymbol{K}_i, \boldsymbol{K}_f$ have no components perpendicular to the scattering plane, it follows that none of the parameters in Eq. (13) depend on the sign of k_y in a frame where the y axis is perpendicular to the scattering plane. The CB1 T-matrix element has the reflection symmetry with respect to the scattering plane given by

$$T_{\boldsymbol{k},1s}^{\mathrm{CB1}}(\theta_k,\varphi_k) = T_{\boldsymbol{k},1s}^{\mathrm{CB1}}(\theta_k, 2\pi - \varphi_k). \tag{14}$$

B. Vortex obtained using the CB1 approximation

We compute the TDCS, in fact a quintuple differential cross section, for inner-shell ionization of carbon according to

$$\frac{d^5\sigma}{d\Omega_f dE_{\boldsymbol{k}} d\Omega_{\boldsymbol{k}}} = (2\pi)^4\frac{2K_f k}{K_i}|T_{\boldsymbol{k},1s}|^2, \tag{15}$$

where $d\Omega_{\boldsymbol{k}}$ is the solid angle for the ejected electron and $d\Omega_f$ is the solid angle for the scattered electron. The factor of two on the right-hand side of this equation is because there are two 1s electrons in the K shell of carbon. We consider only the direct ionization T-matrix element, which is a reasonable approximation since we consider the kinematics where the energy of the ejected electron is much lower than the energy of the incident electron.

In the CB1 TDCS for inner-shell ionization of carbon by electron impact reported by Botero and Macek [28], a minimum is seen at about $\theta_k = 240°$ for the kinematic conditions $E_i = 1801.2$ eV, $\theta_f = 4°$, and $E_{\boldsymbol{k}} = 9.6$ eV. We compute the CB1 T-matrix element for these kinematics and find that while $\mathrm{Im}[T_{\boldsymbol{k},1s}^{\mathrm{CB1}}]$ is 0 at 240°, $\mathrm{Re}[T_{\boldsymbol{k},1s}^{\mathrm{CB1}}]$ is 0 not at this angle, but at 242°. Therefore, the minimum in the TDCS does not occur exactly at the position of a vortex because there is a small part of $\mathrm{Re}[T_{\boldsymbol{k},1s}^{\mathrm{CB1}}]$ where $\mathrm{Im}[T_{\boldsymbol{k},1s}^{\mathrm{CB1}}]$ vanishes. Since $\mathrm{Re}[T_{\boldsymbol{k},1s}^{\mathrm{CB1}}] = 0$ at an angle close to the angle, where $\mathrm{Im}[T_{\boldsymbol{k},1s}^{\mathrm{CB1}}] = 0$ and where there is a minimum in the CB1 TDCS, the minimum in the CB1 TDCS could be explained as being due to a vortex for kinematics close to those where the minimum is obtained. In all the calculations that we report in this section, the energy of the incident electron E_i is 1801.2 eV and the angle of the scattering electron θ_f is 4°.

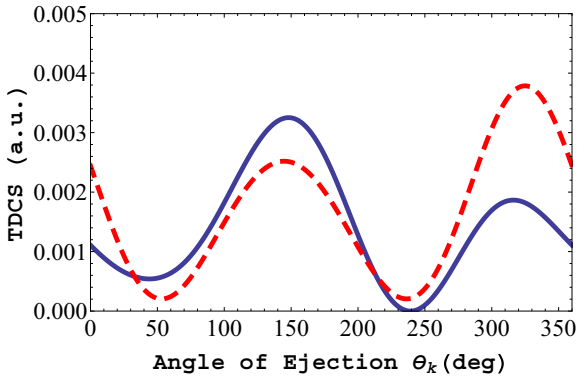

FIG. 1. (Color online) Plot of angular distributions of the TDCS computed in the CB1 [solid (blue) curve] and the B1 [dashed (red) curve] for electron-impact ionization of the K shell of carbon for the kinematic conditions $E_i = 1801.2$ eV, $\theta_f = 4^\circ$, and $E_k = 5.5$ eV.

We systematically vary the energy of the ejected electron E_k to search for where $\mathrm{Re}[T^{\mathrm{CB1}}_{k,1s}] = 0$ at the same angle that $\mathrm{Im}[T^{\mathrm{CB1}}_{k,1s}] = 0$. We find that for $E_k = 5.5$ eV a deep minimum occurs in the CB1 TDCS at the angle of the ejected electron θ_k of 239°, and at this angle $\mathrm{Re}[T^{\mathrm{CB1}}_{k,1s}] = \mathrm{Im}[T^{\mathrm{CB1}}_{k,1s}] = 0$. The deep minimum in the CB1 TDCS is due to a vortex in the velocity field. We also compute the B1 TDCS using Eq. (15) and the closed-form expression of the B1 approximation of Mott and Massey [3]. In Fig. 1, we show the TDCS computed in the CB1 and B1 approximations for $E_k = 5.5$ eV. The deep minimum in the CB1 TDCS is close to the minimum in the B1 TDCS, which is at 236°. This minimum in the B1 TDCS is not deep and does not correspond to a vortex. In Fig. 2 we show the real and imaginary parts of the CB1 ionization T-matrix element for these kinematics.

We show in Fig. 3 a density plot of $\ln|T^{\mathrm{CB1}}_{k,1s}|$ as a function of the x and z components, k_x and k_z, of the momentum of the ejected electron $\boldsymbol{k}$, where the z axis is taken to be the direction of the incident electron. The $x-z$ plane is taken to be the scattering plane. The electron is ejected in the scattering plane, so that the y component of the momentum

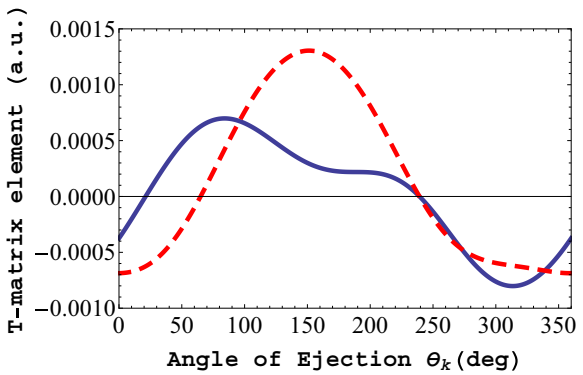

FIG. 2. (Color online) Real [solid (blue) curve] and imaginary [dashed (red) curve] parts of the Coulomb-Born (CB1) ionization T-matrix element for electron-impact ionization of the K shell of carbon under the kinematic conditions $E_i = 1801.2$ eV, $\theta_f = 4^\circ$, and $E_k = 5.5$ eV.

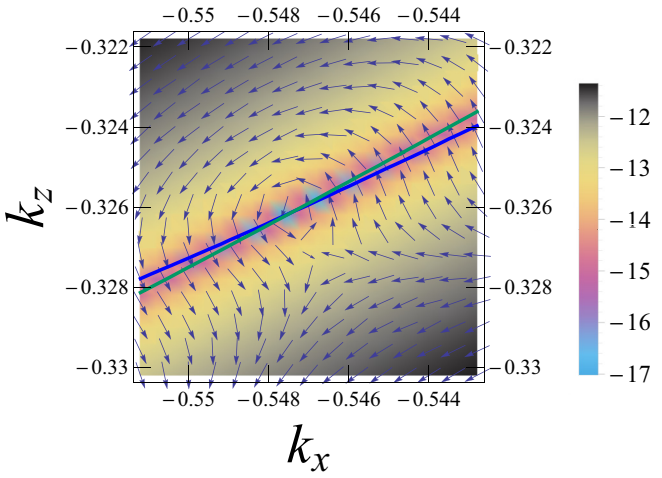

FIG. 3. (Color online) Density plot of $\ln|T^{\mathrm{CB1}}_{k,1s}|$ as a function of the x and z components (k_x, k_z) of momentum $\boldsymbol{k}$ of the ejected electron for electron-impact ionization of the K shell of carbon. The nodal lines where $\mathrm{Re}[T^{\mathrm{CB1}}_{k,1s}] = 0$ and $\mathrm{Im}[T^{\mathrm{CB1}}_{k,1s}] = 0$ are shown by solid blue and green curves, respectively. Arrows show the direction of the velocity field $\boldsymbol{v} = \nabla_k \mathrm{Im}[\ln T^{\mathrm{CB1}}_{k,1s}]$.

of the ejected electron, k_y, is 0. In obtaining Fig. 3, we fix the incident energy E_i and the scattering angle θ_f, while we vary the energies of the ejected and scattered electrons to maintain energy conservation. Also, we show in Fig. 3 the nodal lines of $\mathrm{Re}[T^{\mathrm{CB1}}_{k,1s}]$ and $\mathrm{Im}[T^{\mathrm{CB1}}_{k,1s}]$. The position where the nodal lines cross is the position of the vortex. This position is $\boldsymbol{k} = (-0.547, 0, -0.326)$, which corresponds to $E_k = 5.5$ eV and $\theta_k = 239^\circ$. We also show by arrows in Fig. 3 the direction of the velocity field $\boldsymbol{v} = \nabla_k \mathrm{Im}[\ln T^{\mathrm{CB1}}_{k,1s}]$. Note that the velocity field circulates around the position of the zero of $|T^{\mathrm{CB1}}_{k,1s}(k_x, 0, k_z)|$. The circulation $\Gamma = \int_c \boldsymbol{v} \cdot d\boldsymbol{\ell}$, where the contour c is a closed loop around the zero taken in the counterclockwise direction, does not vanish. We verify that it equals 2π (to numerical accuracy). We conclude that the deep minimum in the CB1 TDCS at $\theta_k = 239^\circ$ for $E_k = 5.5$ eV is due to a vortex in the velocity field.

C. Multipole expansion of the ionization T-matrix element

It is insightful to examine the multipole components in an expansion of the CB1 ionization T-matrix element to investigate the vortex in more detail. We perform a multipole expansion of both the CB1 and the B1 ionization T-matrix elements relative to an axis parallel to the momentum transfer vector $\boldsymbol{K} = \boldsymbol{K}_i - \boldsymbol{K}_f$ for the kinematics of where the vortex is obtained in the CB1 approximation. We follow the treatment of Botero and Macek [28] in obtaining the CB1 and B1 multipole components of the T-matrix element, correcting for some apparent mistakes in the equation given in Ref. [28] for the B1 multipole components. Botero and Macek computed multipole components of the CB1 and B1 T-matrix elements for a number of kinematics including the kinematics where measurements were made of the TDCS [62].

The multipole expansion of the T-matrix element relative to the z' axis parallel to the momentum transfer vector $\boldsymbol{K}$ is

TABLE I. Coulomb-Born (CB1) and Born (B1) multipole components of the T-matrix element for electron-impact ionization of the K shell of carbon for the kinematics that give a vortex ($E_i = 1801.2$ eV, $\theta_f = 4^\circ$, and $E_k = 5.5$ eV). The z' axis is taken parallel to the momentum transfer vector. The phases of the multipole components T_ℓ^m are $\varphi_{\ell m}$, and $\varphi'_{\ell m}$ are the phases of the multipole components T_ℓ^m relative to the phase φ_{10}. Phases are given in degrees.

ℓ	m	$(2\pi)^4 \frac{2K_f k}{K_i} \lvert T_\ell^{m\,(\mathrm{CB1})}\rvert^2$	$\varphi_{\ell m}^{\mathrm{CB1}}$	$\varphi_{\ell m}^{\prime\mathrm{CB1}}$	$(2\pi)^4 \frac{2K_f k}{K_i} \lvert T_\ell^{0\,(\mathrm{B1})}\rvert^2$	$\varphi_{\ell m}^{\mathrm{B1}}$	$\varphi_{\ell m}^{\prime\mathrm{B1}}$
0	0	3.3×10^{-4}	25.8	146	3.25×10^{-4}	−101.2	−277.8
1	0	1.06×10^{-2}	−120.0	0	1.35×10^{-2}	176.6	0
1	1	3.24×10^{-4}	150.6	270.6			
2	0	8.74×10^{-4}	140.4	260.4	9.09×10^{-4}	101.9	−74.7
2	1	2.50×10^{-6}	−45.6	74.4			
2	2	2.94×10^{-6}	74.0	194.0			
3	0	1.67×10^{-5}	56.7	176.7	1.66×10^{-5}	34.1	−142.5
3	1	1.27×10^{-6}	−169.3	−49.3			
3	2	6.27×10^{-7}	7.7	127.7			
3	3	3.30×10^{-8}	−160	−40.1			
4	0	1.61×10^{-7}	−18.3	101.7	1.49×10^{-7}	−27.3	−203.9
4	1	1.05×10^{-8}	103.9	−223.9			
4	2	1.73×10^{-9}	−79.7	40.3			
4	3	3.9×10^{-11}	−65	55			
4	4	3×10^{-11}	120.8	241			

given by

$$T_{fi}(\theta'_k,\varphi'_k) = \sum_{\ell=0}^{\infty} \sum_{m=-\ell}^{\ell} T_\ell^m Y_\ell^m(\theta'_k,\varphi'_k), \tag{16}$$

where θ'_k and φ'_k are, respectively, the polar and azimuthal angles for this z' axis and for the $x'-z'$ plane as the scattering plane. The $Y_\ell^m(\theta'_k,\varphi'_k)$ are the usual complex spherical harmonics. We use the definition of the spherical harmonics given in Ref. [65], which includes the $(-1)^m$ Condon-Shortley factor. The coefficients T_ℓ^m are for an expansion of the T matrix in terms of $Y_\ell^m(\theta'_k,\varphi'_k)$.

Using the orthonormality condition of the spherical harmonics and the property that $T_{fi}(\theta'_k,\varphi'_k)$ is symmetric with respect to φ'_k, one can write

$$T_\ell^m = 2\int_0^\pi \int_0^\pi \mathrm{Re}[Y_\ell^m(\theta'_k,\varphi'_k)] T_{fi}(\theta'_k,\varphi'_k) \sin\theta'_k d\theta'_k d\varphi'_k. \tag{17}$$

Since $T_\ell^{-m} = (-1)^m T_\ell^m$, the multipole expansion, Eq. (16), can be written as

$$T_{fi}(\theta'_k,\varphi'_k) = \sum_{\ell=0}^{\infty} \left(T_\ell^0 Y_\ell^0(\theta'_k,\varphi'_k) + \sum_{m=1}^{\ell} T_\ell^m \left(Y_\ell^m(\theta'_k,\varphi'_k) + (-1)^m Y_\ell^{-m}(\theta'_k,\varphi'_k) \right) \right). \tag{18}$$

In the Appendix we give equations for the B1 ionization T-matrix element and its multipole components. The components given in Ref. [28] apparently have errors. We list in Table I, for the CB1 and B1 approximations, the phases of the components of the T-matrix element for the kinematics of a vortex and the quantity $(2\pi)^4 \frac{2K_f k}{K_i} \lvert T_\ell^m\rvert^2$. The values of the relative phases φ'_{20} and φ'_{11} are important to get a deep minimum in the TDCS, as we discuss following Eq. (20).

In Fig. 4, we compare the TDCS computed using different CB1 multipole components in the expansion of the CB1 ionization T-matrix element for the kinematics of a vortex ($E_k = 5.5$ eV). The various TDCSs are plotted versus the angle of the ejected electron measured relative to the incident beam direction. We consider the electron ejected in the scattering plane. The TDCS we compute with $\ell_{\max} = 3$ CB1 components (not shown) and the TDCS we compute with $\ell_{\max} = 4$ CB1 components (shown) are virtually indistinguishable in the figure and agree very well with the CB1 TDCS we compute with the full CB1 T-matrix element (not shown in Fig. 4). As with the CB1 TDCS, the TDCS we compute with the CB1 components up to $\ell_{\max} = 4$ and all allowed m values has a deep minimum at 239°.

Figure 5 shows the angular distributions of the TDCS for the kinematics of a vortex computed with different multipole components. The z axis shown is parallel to the incident beam direction. The figure illustrates the importance of the CB1

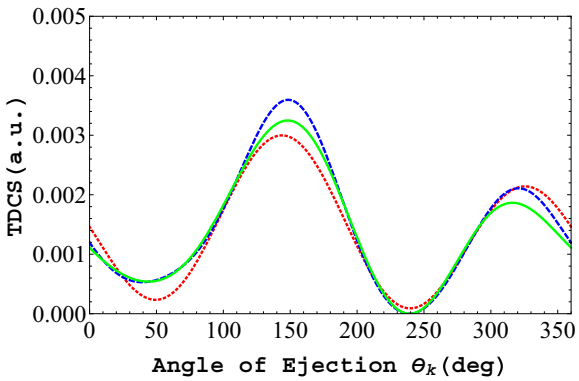

FIG. 4. (Color online) TDCS for K-shell ionization of carbon by electron impact computed using different multipole components in the expansion of the CB1 ionization T-matrix element. Kinematic conditions are $E_i = 1801.2$ eV, $\theta_f = 4^\circ$, and $E_k = 5.5$ eV. The TDCS we compute with $\ell_{\max} = 1$ is shown by the dotted (red curve); that with $\ell_{\max} = 2$, by the dashed (blue) curve; and that with $\ell_{\max} = 4$, by the solid (green) curve.

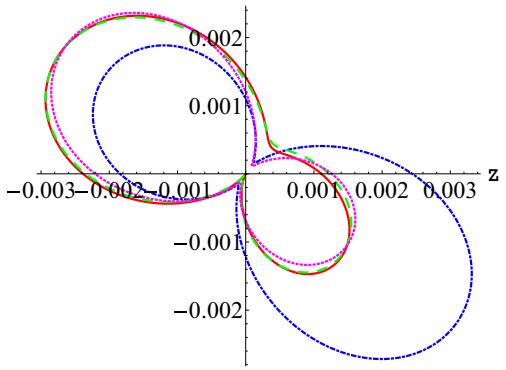

FIG. 5. (Color online) Angular distributions of the TDCS for K-shell ionization of carbon by electron impact. The z axis is parallel to the incident beam direction. The kinematic conditions ($E_i = 1801.2$ eV, $\theta_f = 4^\circ$, and $E_k = 5.5$ eV) are for a vortex. The TDCS computed with the CB1 $\ell = 0 \rightarrow 4$, $-\ell \leqslant m \leqslant \ell$ components is shown by the solid (red) curve; the TDCS computed with the CB1 $\ell_{\max} = 4$, $m = 0$ plus $\ell = 1$, $m = \pm 1$ components, by the long-dashed (green) curve; and the TDCS computed with the CB1 $\ell = 0 \rightarrow 4$, $m = 0$ components, by the dotted (magenta) curve. The TDCS computed with the B1 multipole components $\ell = 0 \rightarrow 4$, $m = 0$ [dot-dashed (blue) curve] is also shown.

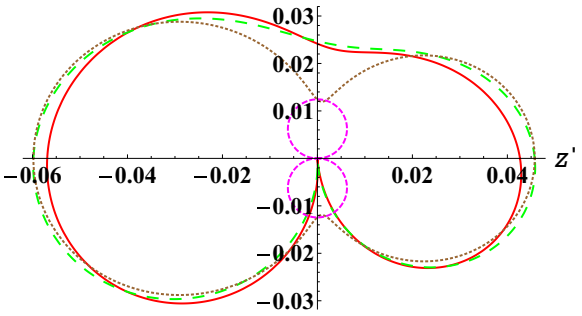

FIG. 6. (Color online) Angular distributions of the TDCS for K-shell ionization of carbon by electron impact. The z' axis is taken parallel to the momentum transfer vector. Kinematic conditions are $E_i = 1801.2$ eV, $\theta_f = 4^\circ$, and $E_k = 5.5$ eV. The TDCS we compute with the CB1 $\ell = 0 \rightarrow 4$, $-\ell \leqslant m \leqslant \ell$ components is shown by the solid (red) curve; the TDCS we compute with the CB1 $\ell = 0 \rightarrow 2$, $m = 0$ plus $\ell = 1$, $m = \pm 1$ components, by the long-dashed (green) curve; the TDCS we compute with the CB1 $\ell = 0 \rightarrow 2$, $m = 0$ components only, by the dotted (brown) curve; and the TDCS we compute with the CB1 $\ell = 1, m = \pm 1$ components, by the dashed (magenta) circles.

$m = \pm 1$ dipole components in obtaining a deep minimum. It shows the TDCS computed with just the CB1 $\ell_{\max} = 4, m = 0$ components, the TDCS computed with CB1 $m = \pm 1$ dipole components added to the CB1 $\ell_{\max} = 4, m = 0$ components of the T-matrix element, and the TDCS computed with the CB1 components with $\ell_{\max} = 4$ and all allowed m values, which is essentially the complete CB1 TDCS. The figure also shows the TDCS computed with the B1 $\ell_{\max} = 4$ components. The TDCS with the B1 $\ell_{\max} = 4$ components is indistinguishable in the figure from the complete B1 TDCS (not shown).

The TDCS we compute with the B1 $\ell_{\max} = 4$ components has a minimum at 236°, close to the deep minimum in the TDCS we compute with the CB1 $\ell_{\max} = 4$ components, which is at 239°. However, the value of the minimum in the TDCS with $\ell_{\max} = 4$ is about 3×10^{-7} smaller than the minimum in the B1 TDCS. The real and imaginary parts of the T-matrix element we compute with the B1 multipole components are not zero at the same angle. The minimum in the B1 TDCS at 236° does not correspond to a vortex in the velocity field.

While there is a deep minimum in the CB1 TDCS, the TDCS we compute using just the CB1 $m = 0$, $\ell_{\max} = 4$ components has a minimum, at about 239°, which is not deep. In the calculation of the T-matrix element using only the $m = 0$, $\ell_{\max} = 4$ components of the CB1 T-matrix element, the angle where $\mathrm{Re}[T_{\boldsymbol{k},1s}] = 0$ is separated quite significantly from the angle where $\mathrm{Im}[T_{\boldsymbol{k},1s}] = 0$. In this case, the minimum in the corresponding TDCS does not correspond to a vortex.

Adding just the CB1 $m = \pm 1$ dipole components to the CB1 $\ell_{\max} = 4$, $m = 0$ components of the T-matrix element makes a huge difference in the shape and magnitude of the TDCS. Adding the CB1 $m = \pm 1$ dipole components brings the angles where $\mathrm{Re}[T_{\boldsymbol{k},1s}] = 0$ and $\mathrm{Im}[T_{\boldsymbol{k},1s}] \approx 0$ close to one another, resulting in a deep minimum in the TDCS at about 237°. Remarkably, the addition of the $m = \pm 1$ CB1 dipole components reduces the value of the minimum in the TDCS by about three orders of magnitude. The $m = \pm 1$ CB1 dipole components are therefore extremely important in obtaining a vortex. Interestingly, the effect of adding the CB1 $m = \pm 1$ dipole components is to increase the value of the minimum that is almost in the opposite direction by a factor of 4. This minimum in the TDCS computed with the CB1 $\ell_{\max} = 4, m = 0$ and $\ell = 1$, $m = \pm 1$ components is at about 47°. In Fig. 5, it is apparent that the angular distribution of the TDCSs we compute using the CB1 $\ell_{\max} = 4$, $m = 0$ and $\ell = 1$, $m = \pm 1$ multipole components is similar to the angular distribution of the TDCS we compute using the complete CB1 TDCS.

The importance of adding the CB1 $m = \pm 1$ dipole components to the $m = 0$ components in reducing the value of one minimum and increasing the value of the other minimum in the TDCS has been presented in Ref. [18]. However, Ref. [18] used different kinematics from those we use in the calculations presented here. Furthermore, in the calculation discussed in Ref. [18], the CB1 $m = \pm 1$ dipole components were added to the B1 components rather than the CB1 $m = 0$ components. Reference [18] commented on the difference in the phase of the ℓ, $m = 0$ components relative to the phase of the $m = 0$ dipole component between the CB1 and the B1 calculations.

Figure 6 gives the angular distribution of the TDCS where the z' axis is parallel to the momentum transfer vector for the kinematics of the vortex ($E_k = 5.5$ eV). For these kinematics, the angle that the momentum transfer vector makes relative to the incident beam direction is approximately 325°. The figure compares the angular distribution of the TDCS that we compute with only the $\ell = 0 \rightarrow 2$, $m = 0$ plus the $\ell = 1$, $m = \pm 1$ CB1 components with that we compute with all the $\ell = 0 \rightarrow 4$, $-\ell \leqslant m \leqslant \ell$ CB1 components, which is essentially the complete CB1 TDCS. It also shows the TDCS that we compute with only the $m = 0$ monopole, dipole, and quadrupole components of the T-matrix element and the TDCS that we compute solely with the $m = \pm 1$ dipole components. It can be seen that the angular distribution of the TDCS we

compute with only the $\ell = 0 \rightarrow 2, m = 0$ plus $\ell = 1, m = \pm 1$ CB1 components is very similar to the angular distribution of the TDCS we compute with the $\ell = 0 \rightarrow 4$, $-\ell \leqslant m \leqslant \ell$ CB1 components. Both angular distributions have a deep minimum at about 270° relative to the momentum transfer axis and a minimum of enhanced magnitude in about the opposite direction (≈90° relative to the momentum transfer axis) compared to the TDCS that we compute with only the $m = 0$ monopole, dipole, and quadrupole components. Thus, from the figure it is evident that the $m = \pm 1$ dipole components are important in obtaining a deep minimum in the TDCS.

It is easier to analyze the T-matrix element that has only the $\ell = 0 \rightarrow 2$, $m = 0$ plus the $\ell = 1$, $m = \pm 1$ components rather than the T-matrix element with $\ell_{\max} = 4$ and all allowed m. This we do below.

D. Analysis of the vortex using the multipole expansion of the ionization T-matrix element

The expansion of the CB1 ionization T-matrix element of Eq. (18) retaining only the $\ell_{\max} = 2$, $m = 0$ plus the $\ell = 1$, $m = \pm 1$ multipole components can be written as

$$T_{fi}(\theta_k',0) = e^{i\varphi_{10}} T'_{fi}(\theta_k',0), \tag{19}$$

where

$$T'_{fi}(\theta_k',0) = \left|T_0^0\right| e^{i\varphi'_{00}} Y_0^0(\theta_k',0) + \left|T_1^0\right| Y_1^0(\theta_k',0) + \left|T_2^0\right| e^{i\varphi'_{20}} Y_2^0(\theta_k',0) + 2\left|T_1^1\right| e^{i\varphi'_{11}} Y_1^1(\theta_k',0) \tag{20}$$

and $\varphi'_{\ell m}$ are the phases of T_ℓ^m relative to the phase of the $m = 0$ dipole component, $\varphi'_{\ell m} = \varphi_{\ell m} - \varphi_{10}$. Since the relative phases φ'_{20} and φ'_{11} are almost 270°, the $m = 0$ quadrupole and the $m = 1$ dipole terms of $T'_{fi}(\theta_k',0)$ are almost purely imaginary. At $\theta_k' = 90°$, the sum of the imaginary parts of the monopole and $m = 0$ quadrupole terms almost equals the imaginary part of the $m = 1$ dipole term (which has the factor of 2 because of the combining of both the $m = 1$ and the $m = -1$ terms). This means that for $\theta_k' = 90°$, adding the $m = \pm 1$ dipole components to the $m = 0$ monopole and quadrupole components almost doubles the magnitude of $\mathrm{Im}[T'_{fi}(\theta_k',0)]$ and also of $T'_{fi}(\theta_k',0)$ itself since $\mathrm{Re}[T'_{fi}(\theta_k',0)] \approx 0$ at $\theta_k' = 90°$. Thus, at an angle of 90° relative to the momentum transfer axis, the TDCS increases by almost a factor of 4 with the inclusion of the $m = \pm 1$ dipole components. However, at $\theta_k' = 270°$, the $m = \pm 1$ dipole components almost cancel with the $m = 0$ monopole and quadrupole components for $\mathrm{Im}[T'_{fi}(\theta_k',0)]$, and because $\mathrm{Re}[T'_{fi}(\theta_k',0)] \approx 0$ at $\theta_k' = 270°$, $T'_{fi}(\theta_k',0)$ and the TDCS are also almost zero at this angle. More terms in the multipole expansion of the T-matrix element are needed for a better cancellation of the T-matrix element at $\theta_k' \approx 270°$, but this analysis illustrates the importance of the $m = 0$ monopole and quadrupole components and the $m = \pm 1$ dipole components for obtaining a deep minimum in the TDCS.

In Ref. [30] a discussion is given of the importance of adding a monopole term to the dipole term to shift the position of the zero in the amplitude from the origin. It is explained in Ref. [30] that an examination of the multipole components of the CB1 T-matrix element determined by Botero and Macek [28] shows that the x component of the ionization amplitude is nearly 90° out of phase with the z component. Reference [30] suggested that the continuum wave function corresponding to the ionization amplitude carries some net angular momentum.

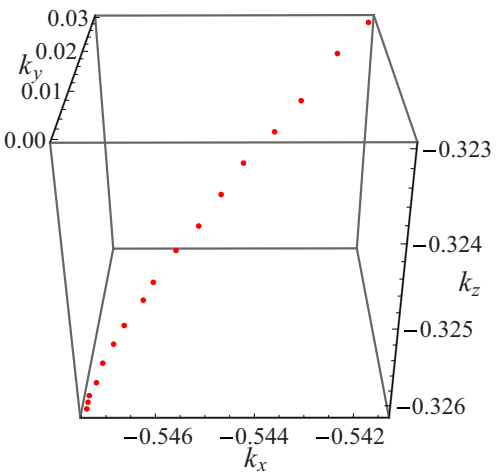

FIG. 7. (Color online) A segment of the vortex line for the K-shell ionization of carbon by electron impact for an incident energy E_i of 1801.2 eV and a scattering angle θ_f of 4°. The positions of the vortex for different values of the y component of the momentum of the ejected electron, k_y, are denoted by filled (red) circles. The loci of the positions of the vortex form a segment of the vortex line.

E. Vortex line

In order to construct a segment of the vortex line for the kinematics of an incident energy $E_i = 1801.2$ eV and scattering angle $\theta_f = 4°$, we also consider the electron from the inner shell of carbon to be ejected out of the scattering plane. We consider a number of different but small values of k_y. For each value of k_y, we vary the values of k_x and k_z, while adjusting the magnitude of $\boldsymbol{K}_f$ to compensate so that the total energy of the system is conserved, and we locate an intersection of the nodal lines of the real and imaginary parts of the CB1 T-matrix element. A point of intersection is a position of a vortex for that particular value of k_y. We repeat this for different fixed small values of k_y. We plot the positions of the vortex points we obtain for different k_y values. The loci of the vortex positions form a segment of the vortex line for the kinematics $E_i = 1801.2$ eV and $\theta_f = 4°$ (see Fig. 7). So that the vortex line is smooth, we use the data on the positions of the vortex points to four significant figures, although we claim an accuracy of the positions to ±0.001 only. The vortex line starts off perpendicular to the scattering plane, the $k_x - k_z$ plane, as it must because of reflection symmetry [17]. However, the vortex line quickly bends towards larger values of k_x and k_z with increasing k_y. The trend of the vortex line, namely, that it appears to start perpendicular to the scattering plane but bends quickly, is similar to that obtained in ion-atom collisions [66].

Expressing the CB1 T-matrix element in terms of the components of the momentum of the ejected electron helps with the understanding of the behavior of the vortex line. The multipole components T_ℓ^m can be written in terms of slowly varying functions $a_{\ell m}(k)$ of k for the energy ranges $E_{\boldsymbol{k}}$ in

Figs. 3 and 7 according to

$$T_\ell^{m\,(\mathrm{CB1})} = (-1)^m (N_{\boldsymbol{k}}^-)^* k^\ell \sqrt{\frac{4\pi}{2\ell+1}}\, a_{\ell m}(k). \tag{21}$$

Substituting Eq. (21) into the multipole expansion, Eq. (16), and retaining only the $m = 0$, $\ell = 0$, 1, and 2, and $\ell = 1, m = 1$ components, which are the most important components in obtaining the vortex, leads to

$$T_{\boldsymbol{k},1s}^{\mathrm{CB1}} \approx (N_{\boldsymbol{k}}^-)^* \big[a_{00} + a_{10} k_z' + a_{20}\big(2k_z'^2 - k_x'^2 - k_y'^2\big)/2 + \sqrt{2} a_{11} k_x'\big]. \tag{22}$$

In Eq. (22) k_x', k_y', and k_z' are the components of the momentum of the ejected electron in which the z' axis is taken parallel to the momentum transfer vector and the x' axis is in the scattering plane.

Using Eq. (22) it can be seen that the vortex line where both $\mathrm{Re}[T_{\boldsymbol{k},1s}^{\mathrm{CB1}}] = 0$ and $\mathrm{Im}[T_{\boldsymbol{k},1s}^{\mathrm{CB1}}] = 0$ is an even function of k_y' and the vortex line is symmetric with respect to the scattering plane. We note in connection with Eq, (22) that Feagin [11] recently developed a threshold-like analytic expression for the scattering amplitude using cylindrical partial waves for the two outgoing electrons about the vortex.

IV. SUMMARY

Using the CB1 approximation, we show that there is a vortex in the velocity field for K-shell ionization of carbon by electron impact for the kinematic conditions $E_i = 1801.2$ eV, $\theta_f = 4^\circ$, $E_{\boldsymbol{k}} = 5.5$ eV, and $\theta_k = 239^\circ$. These kinematics are close to the conditions where a minimum was found in experiments [62] and in earlier calculations [28]. For this process, we give a plot of the nodal lines of $\mathrm{Re}[T_{\boldsymbol{k},1s}^{\mathrm{CB1}}] = 0$ and $\mathrm{Im}[T_{\boldsymbol{k},1s}^{\mathrm{CB1}}] = 0$ showing the point where they cross, a plot of the velocity field associated with $T_{\boldsymbol{k},1s}^{\mathrm{CB1}}$ showing that the velocity field circulates around the point where $\mathrm{Re}[T_{\boldsymbol{k},1s}^{\mathrm{CB1}}] = \mathrm{Im}[T_{\boldsymbol{k},1s}^{\mathrm{CB1}}] = 0$, and verification that circulation along a closed contour encircling this point cross gives 2π. Our work verifies that there is a vortex in the velocity field associated with the T-matrix element for electron ionization. We also determine a segment of the vortex line for the kinematics $E_{\mathrm{i}} = 1801.2$ eV and $\theta_f = 4^\circ$. The line starts off perpendicular to the scattering plane due to reflection symmetry. Furthermore, we give a detailed analysis of the partial-wave expansion of the CB1 ionization T-matrix element for the kinematics of the vortex and demonstrate the importance of the $m = \pm 1$ dipole components in producing the zero in $T_{\boldsymbol{k},1s}^{\mathrm{CB1}}$.

ACKNOWLEDGMENTS

We appreciate discussions with Dr. S. Yu. Ovchinnikov and Dr. D. R. Schultz. We are thankful to Dr. Javier Botero for providing us his Coulomb-Born and Born Fortran codes. S.J.W. acknowledges support from the NSF under Grant No. PHYS-0968638 and from the UNT through UNT Faculty Research Grant No. GA9150. J.H.M. acknowledges support by the DOE. under Grant No. DE-FG02-02ER15283.

APPENDIX: A MULTIPOLE EXPANSION OF THE BORN IONIZATION T-MATRIX ELEMENT

We give the B1 approximation to the ionization T-matrix element and its components in a multipole expansion. These were given in Ref. [28], but there appears to be some mistakes there.

The B1 approximation to the T-matrix element is given by [28]

$$T_{fi}^{\mathrm{B1}} = \langle \Phi_{\boldsymbol{K}_f}(\boldsymbol{r}) \psi_{\boldsymbol{k}}^-(\boldsymbol{r}') \left| \frac{1}{|\boldsymbol{r} - \boldsymbol{r}'|} \right| \varphi_i(\boldsymbol{r}') \Phi_{\boldsymbol{K}_i}(\boldsymbol{r}) \rangle, \tag{A1}$$

where $\Phi_{\boldsymbol{K}_i}(\boldsymbol{r})$ and $\Phi_{\boldsymbol{K}_f}(\boldsymbol{r})$ are the plane waves for the incident electron and the scattered electron normalized to the momentum scale. The integration with respect to $\boldsymbol{r}$, where $\boldsymbol{r}$ is the position vector of the incident (scattered) electron, can easily be performed, allowing T_{fi}^{B1} to be written as

$$T_{fi}^{B1} = \frac{4\pi}{(2\pi)^3 K^2} \langle \psi_{\boldsymbol{k}}^-(\boldsymbol{r}') | e^{i\boldsymbol{K}\cdot\boldsymbol{r}'} \varphi_i(\boldsymbol{r}') \rangle, \tag{A2}$$

where $\boldsymbol{K} = \boldsymbol{K}_i - \boldsymbol{K}_f$ is the momentum transfer vector. Equation (A2) is in agreement with Eq. (B1) of Botero and Macek [28]. Taking $\varphi_i(\boldsymbol{r}')$ for the inner $1s$ electron of carbon to be a ground-state hydrogenic wave function and using the function I_{ab} given in Ref. [39] enables the B1 T-matrix element to be expressed as

$$T_{fi}^{\mathrm{B1}} = -\frac{1}{(2\pi)^3} \frac{4\pi}{K^2} (N_k^-)^* \frac{Z^{3/2}}{\sqrt{\pi}} \frac{\partial}{\partial x} I_{0c} \Big|_{x=Z_T}, \tag{A3}$$

where

$$I_{0c} = \int e^{i(\boldsymbol{K}-\boldsymbol{k}')\cdot\boldsymbol{r}} \frac{e^{-xr}}{r} {}_1F_1[c, 1; i(k'r + \boldsymbol{k}'\cdot\boldsymbol{r})] d\boldsymbol{r} = \frac{4\pi C^{c-1}}{A^c}, \tag{A4}$$

in which $C = x^2 + (\boldsymbol{K} - \boldsymbol{k}')^2$ and $A = (x - ik')^2 + K^2$. Equation (A3) contains an extra factor of $-(2\pi)^{-3/2}$ compared to Eq. (B2) in Ref. [28].

In the B1 approximation, only the $m = 0$ multipole components of the expansion of the T-matrix element Eq. (16), where the z' axis is taken parallel to $\boldsymbol{K}$, are nonzero. They are given by

$$T_\ell^{\mathrm{B1}} = (2\pi) \sqrt{\frac{2\ell+1}{4\pi}} \int_{-1}^{1} T_{fi} P_\ell(y) dy, \tag{A5}$$

where $y = \cos\theta$. Using Eq. (A3) in Eq. (A5) gives, for the B1 $m = 0$ multipole components,

$$T_\ell^{\mathrm{B1}} = -\frac{4(N_k^-)^* Z^{5/2} \sqrt{2\ell+1}}{\pi K^2 [(Z - ik)^2 + K^2]^c} \times \left[(c-1) f_\ell(c-2) - \frac{(c+1)}{[(Z-ik)^2 + K^2]} f_\ell(c-1) \right], \tag{A6}$$

where $f_\ell(\gamma)$, defined in Eq. (B5) in Ref. [28], is

$$f_\ell(\gamma) = \int_{-1}^{1} (Z^2 + q^2 + k^2 - 2qky)^\gamma P_\ell(y) dy. \tag{A7}$$

Equation (A6) for T_ℓ^{PBA} corrects for mistakes found in Eqs. (64) and (B4) in Ref. [28].

Following the procedure given in Ref. [28], i.e., using Rodrigue's formula for the Legendre polynomial and integration by parts ℓ times, gives

$$f_\ell(\gamma) = \frac{\ell!\Gamma[1+\gamma]2^{\ell+1}(Z^2+(K-k)^2)^{\gamma-\ell}(-2kK)^\ell}{(2\ell+1)!\Gamma[1+\gamma-\ell]}\,{}_2F_1\left[\ell+1,\ell-\gamma;2\ell+2,\frac{-4kK}{Z^2+(K-k)^2}\right]. \tag{A8}$$

This equation corrects mistakes in Eqs. (65) and (B5) in Ref. [28].

[1] U. Fano, Annu. Rev. Nucl. Sci. **13**, 1 (1963).
[2] M. Inokuti, Rev. Mod. Phys. **43**, 297 (1971).
[3] N. F. Mott and H. S. W. Massey, in *The Theory of Atomic Collisions* (Oxford University Press, London, 1965), p. 489.
[4] J. S. Briggs, Comments At. Mol. Phys. **23**, 155 (1989).
[5] A. J. Murray and F. H. Read, J. Phys. B **26**, L359 (1993).
[6] A. J. Murray and F. H. Read, Phys. Rev. A **47**, 3724 (1993).
[7] J. Berakdar and J. S. Briggs, J. Phys. B **27**, 4271 (1994).
[8] J. Berakdar and J. S. Briggs, Phys. Rev. Lett. **72**, 3799 (1994).
[9] J. H. Macek, J. B. Sternberg, S. Yu. Ovchinnikov, and J. S. Briggs, Phys. Rev. Lett. **104**, 033201 (2010).
[10] J. Colgan, O. Al Hagan, D. H. Madison, A. J. Murray, and M. S. Pindzola, J. Phys. B **42**, 171001 (2009).
[11] J. M. Feagin, J. Phys. B **44**, 011001 (2011).
[12] T.-G. Lee, S. Yu. Ovchinnikov, J. Sternberg, V. Chupryna, D. R. Schultz, and J. H. Macek, Phys. Rev. A **76**, 050701(R) (2007).
[13] J. H. Macek, J. B. Sternberg, S. Y. Ovchinnikov, T.-G. Lee, and D. R. Schultz, Phys. Rev. Lett. **102**, 143201 (2009).
[14] J. H. Macek, in *Dyanamical Processes in Atomic and Molecular Physics*, edited by G. Ogurtsov and D. Dowek (Bentham Science, Sharjah, UAE, 2012), Chap. 1, p. 3.
[15] D. R. Schultz, J. H. Macek, J. B. Sternberg, S. Yu. Ovchinnikov, and T.-G. Lee, J. Phys.: Conf. Ser. **194**, 082003 (2009); **194**, 012041 (2009).
[16] S. Y. Ovchinnikov, J. H. Macek, J. S. Sternberg, T.-G. Lee, and D. R. Schultz, AIP Conf. Proc. **1099**, 164 (2009).
[17] J. H. Macek, J. Phys.: Conf. Ser. **212**, 012008 (2010).
[18] J. H. Macek, AIP Conf. Proc. **1336**, 138 (2011).
[19] S. Y. Ovchinnikov, J. H. Macek, L. Ph. H. Schmidt, and D. R. Schultz, Phys. Rev. A **83**, 060701(R) (2011).
[20] D. R. Schultz, S. Y. Ovchinnikov, J. B. Sternberg, and J. H. Macek, AIP Conf. Proc. **1336**, 123 (2011).
[21] S. Yu. Ovchinnikov, J. H. Macek, and D. R. Schultz (unpublished) (2014).
[22] L. Ph. H. Schmidt, C. Goihl, D. Metz, H. Schmidt-Böcking, R. Dörner, S. Yu. Ovchinnikov, J. H. Macek, and D. R. Schultz, Phys. Rev. Lett. **112**, 083201 (2014).
[23] F. Navarrete, R. Della Picca, J. Fiol, and R. O. Barrachina, in *Programme and Book of Abstracts, 16th International Workshop on Low-Energy Positron and Positronium Physics* (National University of Ireland, Maynooth, Ireland, 2011), p. 69.
[24] F. Navarrete, R. Della Picca, J. Fiol, and R. O. Barrachina, J. Phys. B **46**, 115203 (2013).
[25] R. Della Picca, J. Fiol, and R. O. Barrachina, Nucl. Instrum. Methods B **233**, 270 (2005).
[26] S. Yu. Ovchinnikov, J. B. Sternberg, J. H. Macek, T.-G. Lee, and D. R. Schultz, Phys. Rev. Lett. **105**, 203005 (2010).
[27] K. G. Lagoudakis, M. Wouters, M. Richard, A. Bass, I. Carusotto, R. André, L. S. Dang, and B. Deveaud-Plédran, Nat. Phys. **4**, 706 (2008).
[28] J. Botero and J. H. Macek, Phys. Rev. A **45**, 154 (1992).
[29] S. J. Ward and J. H. Macek, http://meetings.aps.org/link/BAPS.2011.DAMOP.Q1.63; http://meetings.aps.org/link/BAPS.2013.GEC.HW1.19; Bull. Am. Phys. Soc. **58**, 61 (2013); http://meetings.aps.org/link/BAPS.2014.DAMOP.Q1.37; http://meetings.aps.org/link/BAPS.2014.GEC.MW1.7
[30] J. H. Macek, AIP Conf. Proc. **1525**, 111 (2013).
[31] I. Bialynicki-Birula, Z. Bialynicka-Birula, and C. Sliwa, Phys. Rev. A **61**, 032110 (2000).
[32] A. L. Fetter, Phys. Rev. **151**, 100 (1966).
[33] W. Henneberg, Z. Phys. **86**, 592 (1933).
[34] M. S. Livingston and H. A. Bethe, Rev. Mod. Phys. **9**, 245 (1937).
[35] J. S. Briggs, J. Phys. B **10**, 3075 (1977).
[36] J. Macek, Phys. Rev. A **37**, 2365 (1988).
[37] J. H. Macek and K. Taulbjerg, J. Phys. B **22**, L523 (1989).
[38] J. S. Briggs and J. H. Macek, Adv. Atom. Mol. Opt. Phys. **28**, 1 (1990).
[39] S. D. Oh, J. H. Macek, and E. Kelsey, Phys. Rev. A **17**, 873 (1978).
[40] N. F. Mott, Proc. Cambr. Philos. Soc. **27**, 553 (1931).
[41] M. E. Rudd and J. H. Macek, Case Studies Atom. Phys. **3**, 47 (1974).
[42] U. Fano and J. H. Macek, Rev. Mod. Phys. **45**, 553 (1973).
[43] J. Macek and D. H. Jaecks, Phys. Rev. A **4**, 2288 (1971).
[44] H. Kleinpoppen and J. F. Williams, eds., *Coherence and Correlation in Atomic Collisions* (Plenum Press, New York, 1980).
[45] N. Andersen, J. T. Broad, E. E. B. Campbell, J. W. Gallagher, and I. V. Hertel, Phys. Rep. **278**, 107 (1997).
[46] K.-K. Kan and J. J. Griffin, Phys. Rev. C **15**, 1126 (1977).
[47] S. K. Ghosh and B. M. Deb, Phys. Rep. **92**, 1 (1982).
[48] J. O. Hirschfelder, A. C. Christoph, and W. E. Palke, J. Chem. Phys. **61**, 5435 (1974).
[49] J. O. Hirschfelder, C. J. Goebel, and L. W. Bruch, J. Chem. Phys. **61**, 5456 (1974).
[50] W. Wilhelm, Phys. Rev. D **1**, 2278 (1970).
[51] J. O. Hirschfelder, J. Chem. Phys. **67**, 5477 (1977).
[52] P. A. M. Dirac, Proc. Roy. Soc. A **133**, 60 (1931).
[53] I. Bialynicki-Birula and Z. Bialynicki-Birula, Phys. Rev. D **3**, 2410 (1971).
[54] P. G. Saffman, *Vortex Dynamics* (Cambridge University Press, Cambridge, 1992).
[55] E. Madelung, Z. Phys. **40**, 322 (1927).
[56] T. Takabayasi, Prog. Theor. Phys. **8**, 143 (1952).
[57] E. C. Kemble, in *The Fundamental Principles of Quantum Mechanics with Elementary Applications* (Dover Publication, Inc., New York, 1958), pp. 58–63.

[58] J. S. Briggs and J. M. Feagin, J. Phys. B **46**, 025202 (2013), and references therein.
[59] J. M. Feagin and J. S. Briggs, J. Phys. B **47**, 115202 (2014).
[60] J. S. Briggs and J. M. Feagin, Phys. Rev. A **90**, 052712 (2014).
[61] J. D. Dollard, Rocky Mt. J. Math. **1**, 5 (1971).
[62] L. Avaldi, R. Camilloni, and G. Stefani, Phys. Rev. A **41**, 134 (1990).
[63] K.-N. Huang, M. Aoyagi, M. H. Chen, B. Crasemann, and H. Mark, Atom. Data Nucl. Data Tables **18**, 243 (1976).
[64] C. J. Joachain, *Quantum Collision Theory*, 3rd ed. (North-Holland, Amsterdam, 1983).
[65] G. B. Arfken and H. J. Weber, *Mathematical Methods for Physicists*, 6th ed. (Elsevier Academic Press, Amsterdam, 2005).
[66] S. Yu. Ovchinnikov, D. R. Schultz, and J. H. Macek (unpublished) (2013).